PLGA nanoparticles embedding molybdenum cluster salts: Influence of chemical composition on physico-chemical properties, encapsulation efficiencies, colloidal stabilities and in vitro release

G Dollo, Y Boucaud, M Amela-Cortes, Y Molard, Stéphane Cordier, N Brandhonneur

PLGA nanoparticles embedding molybdenum cluster salts: influence of chemical composition on physico-chemical properties, encapsulation efficiencies, colloidal stabilities and *in vitro* release

Dollo G.[a,b*], Boucaud Y.[a], Amela-Cortes M.[a], Molard Y.[a],

Cordier S.[a] and Brandhonneur N.[a]

[a] Univ Rennes, ISCR (Institut des Sciences Chimiques de Rennes) – UMR 6226, F-35000, Rennes, France.

[b] CHU de Rennes, Pôle Pharmacie, F-35033 Rennes, France.

[*] Corresponding author:

Dr Gilles Dollo

Faculté des Sciences Pharmaceutiques et Biologiques

2, avenue du Pr Léon Bernard, 35043 Rennes France

Tel: +33 2 23 23 48 02

Email:gilles.dollo@univ-rennes1.fr

*Graphical Abstract (for review)

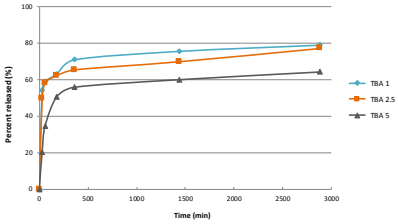

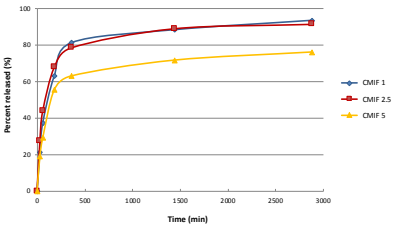

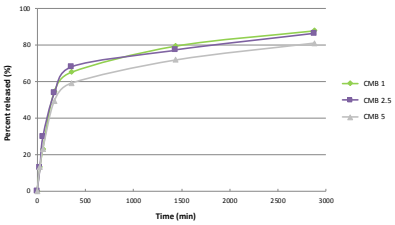

365 nm

Characterizations

	Size (nm)	PDI	Zeta Potentiel (mV)
TBA_2 - PLGA[a]	85.7 ± 4.9	0.12 ± 0.02	-25.8 ± 4.4
CMIF - PLGA[a]	102.0 ± 2.6	0.16 ± 0.01	-38.2 ± 1.7
CMB - PLGA[a]	75.7 ± 2.5	0.16 ± 0.02	-22.4 ± 9.8
TBA_2 - PLGA[b]	95.0 ± 6.1	0.12 ± 0.01	-42.2 ± 8.0
CMIF - PLGA[b]	124.7 ± 2.5	0.08 ± 0.02	-47.8 ± 4.6
CMB - PLGA[b]	99.3 ± 4.6	0.12 ± 0.01	-47.8 ± 9.1
TBA_2 - PLGA[c]	141.7 ± 6.4	0.09 ± 0.02	-24.8 ± 1.3
CMIF - PLGA[c]	144.7 ± 4.7	0.09 ± 0.03	-31.5 ± 3.6
CMB - PLGA[c]	118.3 ± 4.3	0.12 ± 0.01	-43.1 ± 6.5

P/C ratio **a)** 1; **b)** 2.5 and **c)** 5

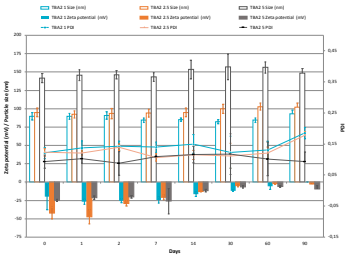

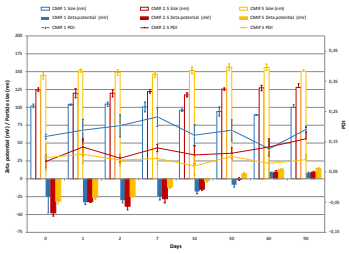

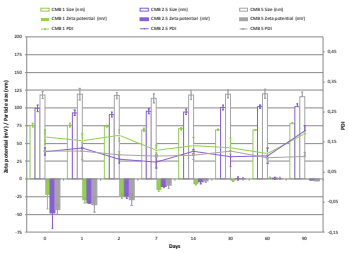

ABSTRACT

We present a screening of poly (D,L-lactide-co-glycolide) (PLGA) nanoparticles embedding a series of inorganic molybdenum octahedral clusters intended for photodynamic therapy (PDT) of cancer. Three cluster compounds from 2 cluster units, $[\{Mo_6Br\}_8Br_6]^{2-}$ and $[\{Mo_6I_8\}(OOC_2F_5)_6]^{2-}$ were studied. $[\{Mo_6Br\}_8Br_6]^{2-}$cluster units are found in the soluble ternary salt $Cs_2[\{Mo_6Br\}_8Br_6]$ (CMB) prepared by solid state chemistry at high temperature. In solution Cs^+ cations are replaced by tetrabutyl ammonium cations $(C_4H_9)_4N^+$) to form the salt $((C_4H_9)_4N)_2[\{Mo_6Br\}_8Br_6]$ (TBA_2). $[\{Mo_6I_8\}(OOC_2F_5)_6]^{2-}$ was prepared combining solid state and solution chemistries; it is paired with Cs^+ cations to form $Cs_2[\{Mo_6I_8\}(OOC_2F_5)_6]$ (CMIF). All tested cluster-based salts could efficiently be incorporated in PLGA nanoparticles as seen with encapsulation efficiencies always higher than 60%. Cluster loaded nanoparticles (CNPs) freshly prepared by solvent displacement method showed spherical shapes, zeta potential values between -20 and -47mV, polydispersity index in the range 0.123-0.167 and sizes in the range 75-150 nm according to the cluster compound and the polymer-to-cluster mass ratio (P/C), suggesting a good cellular uptake. CNPs colloidal stability was maintened for 3 months when they were stored refrigerated and protected from light but the chemical stability was shorter, i.e. 4 weeks, 1 week and 1 day for CMIF, TBA2 and CMB, respectively, CMIF penta-fluoropropionate apical ligands being less rapidly substituted by hydroxyles groups than TBA_2 and CMB halogen apical ligands. FT-IR analysis revealed the lack of strong chemical interaction between cluster compounds and polymer within the nanoparticles. An interesting quick cluster *in vitro* release driven by diffusion outside the nanoparticles porous matrix was observed for all cluster compounds when P/C ratio was ≤ 2.5 and only a higher P/C ratio not studied in this work (i.e > 5) could significantly affect the release of the encapsulated cluster compound. Photophysical properties of cluster compounds were preserved following PLGA incorporation. This work presents PLGA nanoparticles as a stable and efficient cluster compound delivery systems for further *in vitro* and *vivo* evaluations in cancer models.

Key words: PLGA nanoparticle, molybdenum cluster, physico-chemical properties, colloidal stability, chemical stability, *in vitro* release.

1. INTRODUCTION

Hexanuclear cluster of molybdenum with the general formula $[Mo_6(L^i)_8(L^a)_6]^{2-}$ (Figure 1) have been widely studied due to their photo-physical and photo-chemical properties (Jackson et al., 1996; Kirakci et al., 2012; Costuas et al., 2015; Dierre et al., 2017). In these clusters, inner ligands (L^i) are halogen atoms (Br, I, Cl) covalently attached to Mo, forming the stable $\{Mo_6L^i_8\}^{4+}$ cluster core, while terminal or apical ligands (L^a) are labile inorganic or organic ligands that are able to affect the physico-chemical properties of the cluster compound. When they are photo-activated near 365 nm, the very highly chemical and photo-stable cluster cores $\{Mo_6L^i_8\}^{4+}$ show bright photoluminescence with broad emission spectra in the red and near-infrared regions (from 550 to 900 nm) with high quantum yields (Vorotnikov et al., 2017; Kirakci et al., 2012; Efremova et al., 2016). When the photo-activation occurs in the presence of oxygen, they can act as powerful photosensitizers generating singlet oxygen efficiently (Kirakci et al., 2012; Jackson et al., 1990; Amela-Cortes et al., 2015). Such physical and chemical properties make molybdenum cluster compounds very attractive in many biological sciences applications such as bioimaging, biolabeling, diagnostics, cell destructing or antimicrobial agents (Vorotnikova et al., 2019; Solovieva et al., 2016; Neaime et al., 2016). As a result, hexanuclear molybdenum halide cluster complexes are potential candidates for theranostic applications (Ahmed et al., 2012). Because of the poor solubility and stability of these cluster compounds in water, the most physiological solvent for biological applications, there is a need to incorporate them into biocompatible delivery systems such as polymeric nanoparticles that will improve the cluster compound i) apparent solubility, ii) protection against hydrolysis and iii) release in tumor areas. Several works have reported the use of water soluble hybrid materials of molybdenum clusters (Kirakci et al., 2016; Svezhentseva et al., 2017) or the encapsulation of molybdenum cluster compounds in matrixes less biocompatible for parenteral injection such as silica nanoparticles (Aubert et al., 2013; Solovieva et al., 2016) or nano-sized polystyrene beads (Vorotnikova et al., 2017). In a previous work our team has shown the feasibility of incorporating a molybdenum cluster compound into poly (D,L-lactide-co-glycolide) (PLGA) nanoparticles to maintain their intrinsic photophysical properties and to use them as photosensitizer after entering the ovarian cancer cells leading to their destruction (Brandhonneur et al., 2018). Nevertheless, the activity and stability of the formulation can be improved by selecting the most appropriate cluster compound and by an optimization of the polymer-to-cluster mass ratio (P/C). The aim of the present study was to prepare PLGA nanoparticles (NPs) embedding a series of inorganic

hexanuclear molybdenum cluster compounds intended for PDT of ovarian cancer and to select the most stable and efficient association for further *in vitro* and in vivo studies. The polymeric nanoparticles were tested as a carrier system for molybdenum cluster compounds to circumvent their poor aqueous solubility. Three cluster compounds from 2 cluster units, $[\{Mo_6Br\}_8Br_6]^{2-}$ and $[\{Mo_6I_8\}(OOC_2F_5)_6]^{2-}$ were studied. $[\{Mo_6Br\}_8Br_6]^{2-}$ cluster units are found in the soluble ternary salt $Cs_2[\{Mo_6Br\}_8Br_6]$ (CMB) prepared by solid state chemistry at high temperature. In solution Cs^+ cations are replaced by tetrabutyl ammonium cations $(C_4H_9)_4N^+$) to form the salt $((C_4H_9)_4N)_2[\{Mo_6Br\}_8Br_6]$ (TBA_2). $[\{Mo_6I_8\}(OOC_2F_5)_6]^{2-}$ was prepared combining solid stae and solution chemistries; it is paired with Cs^+ cations to form $Cs_2[\{Mo_6I_8\}(OOC_2F_5)_6]$ (CMIF). These cluster compounds loaded nanoparticles (CNPs) were prepared by solvent displacement method using polysorbate 20 as stabilizer and carboxylic acid terminated poly (D,L-Lactide-co-glycolide) (PLGA) polymer with a 50:50 lactide to gycolide ratio. Several polymer-to-cluster mass ratios (P/C) were tested, 1, 2.5 and 5. CNPs were characterized using transmission electron microscopy or TEM (size and shape), dynamic light scattering or DLS (size, polydispersity index, zeta potential, colloidal stability over 3 months), Fourier transform infrared spectroscopy or FT-IR (cluster/polymer interactions), UV spectroscopy (encapsulation efficiency or EE, drug loading or DL, water stability and drug release behavior). Finally, the effect of PLGA nanoparticles incorporation on cluster compound photochemical parameters that can influence the generation of oxygen singlet, i.e. absolute quantum yields and maximum emission wavelengths, were evaluated.

2. MATERIAL AND METHODS

2.1. Chemicals

CMB was synthesized by solid state reaction techniques at high temperature whereas TBA_2 and CMIF were prepared by combining solid state reactions and solution chemistry routes in our laboratory (ISCR, CSM, Rennes, France) using reported procedures (Kirakci et al., 2005, Amela-Cortes et al., 2015). Acid terminated PLGA with a 50:50 lactide to gycolide ratio, MW 24000-38000 (Resomer® RG503H) and polyoxyethylenesorbitan monolaurate or polysorbate 20 (Tween® 20) were purchased from Sigma Aldrich (St Louis, MO, USA). Analytical reagent grade acetone, acetonitrile and absolute ethanol were obtained from VWR international S.A.S. (Fontenay-sous-bois, FR).

2.2. Nanoparticles preparation

CNPs and cluster free nanoparticles or blank nanoparticles were prepared by solvent displacement method or nanoprecipitation, described by Fessi et al. (1989). An organic solution of PLGA polymer (10 to 50 mg) and cluster compound (9-13 mg according to its molecular weight) in acetone (5 ml) was slowly added dropwise (1 ml/min) to a 0.5% w/v aqueous polysorbate 20 solution (15 ml) with a 5 ml syringe and a 25G (0.5mm x 16 mm) needle (Terumo Europe, Leuven, Belgium) under magnetic stirring (500 rpm) at room temperature (20-25°C°). In these conditions, a bluish colloidal nanosuspension was instantaneously formed owing to the ouzo effect (Francois et al., 2005). The acetone was then removed under reduced pressure (200 mbar) by a rotary evaporator Laborata 4000 (Heidolph, Schwabach, Germany) for 1h. The nanosuspensions (≃ 15 ml) were then purified by a first step of centrifugation (5000 g / 5 min) to eliminate polymer aggregates and by a second step of dialysis against 1 liter of deionized water for 1h to eliminate free cluster, using Spectra/Por®6 pre-wetted dialysis membrane with a molecular weight cut-off of 25kD (Spectrum Laboratories, Inc, Rancho Dominguez, CA, USA). The resulting nanosuspensions were used for size, PDI and zeta potential determinations, encapsulation efficiency, cluster loading, water stability evaluation, release studies and quantum yields measurements. CNPs physico-chemical characterizations performed in solid state, such as FT-IR, quantum yields and emission spectra needed a freeze-drying stage of cluster loaded nanosuspensions for 24 h using a Christ®Alpha laboratory freeze-drier, (Martin Christ, Germany).

2.3. Nanoparticles characterization

2.3.1. Particles size, polydispersity index and zeta potential

All three CNPs mean hydrodynamic diameters (nm) and polydispersity indexes (PDI) were determined by laser dynamic light scattering (DLS), and their zeta potentials (mV) were determined by laser droppler micro-electrophoresis technique using Malvern Zetasizer Nano ZS (Malvern Instruments, Malvern, United Kingdom). For each CNPs, all measurements were carried out in triplicate (from 3 different batches) following appropriate sample dilution with distilled water, immediately after preparation and following 1, 2, 7, 14, 30, 60 and 90 days storage protected from light, at room temperature and refrigerated between +2 and +8°C.

2.3.2. Encapsulation efficiency, cluster loading and mass yield

Cluster compounds encapsulation efficiency (EE%) as well as cluster compounds loading in polymeric nanoparticles (CL%) were determined by UV spectroscopy at 250 nm following appropriate dilution with acetonitrile (Specord®PC 205 UV VIS spectrophotometer, Analytik Jena AG, Jena, Germany). Cluster calibration curve was linear from 2 to 20 µg/ml (r^2 = 0.99991). Encapsulation efficiency determinations were performed immediately after preparation following centrifugation of the CNPs suspensions at 40000 *g* for 30 min (Sigma 3K20 high speed refrigerated centrifuge). Free or non-encapsulated cluster compounds were collected from supernatant, diluted with acetonitrile and concentrations were determined by UV spectroscopy at 250 nm.

EE or the ratio of the experimental percent cluster loaded in the polymeric nanoparticles to the initial amount of cluster in the formulation was calculated according the following equation:

$$\text{EE}\ (\%) = \frac{\text{initial cluster amount (mg)} - \text{non encapsulated cluster (mg)}}{\text{initial cluster amount (mg)}} \text{ x } 100$$

Cluster loading (CL %) was performed by centrifugation of the CNPs suspension at 40000 *g* for 30 min followed by freeze-drying of the sediment for 24h, after re-dispersion in distilled water. A known amount of CNPs close to 5 mg was dissolved in 2 ml acetonitrile, diluted (1/50) with acetonitrile and assayed for cluster quantification using the previous UV method. CL or the percent cluster in the freeze dried polymeric nanoparticles was calculated according the following equation:

$$\text{CL}(\%) = \frac{\text{encapsulated cluster in freeze dried nanoparticles (mg)}}{\text{freeze dried nanoparticles amount (mg)}} \text{ x } 100$$

Mass yields (MY%) of the formulations were also determined using the equation:

$$\text{MY}(\%) = \frac{\text{purified freeze dried nanoparticles amount (mg)}}{\text{initial freeze dried nanoparticles amount (mg)}} \text{ x } 100$$

2.3.3. Transmission Electron Microscopy (TEM)

CNPs morphologies were examined with a transmission electron microscope (TEM, JEOL 2100, Japan) and charge coupled device camera Orius 200D (GatanInc, Pleasanton, USA). Samples were prepared by placing a drop of CNPs nanosuspensiononto a carbon coated copper grid and air-dried, following negative staining during 3 min with one drop of 2%

aqueous solution of uranyl acetate for contrast enhancement. The air-dried samples were then directly examined under the transmission electronic microscope.

2.3.4. Fourier Transform Infrared Spectroscopy (FT-IR)

PLGA Polymer (RG503H), cluster compounds TBA_2, CMB and CMIF, freeze dried blank nanoparticles, freeze dried CNPs as well as physical mixtures between cluster compounds and polymer with P/C ratios of 1, 2.5 and 5 were all analyzed by infrared spectroscopy using Universal Attenuated Total Reflectance Accessory (UATRA) Spectrum Two™ FT-IR Spectroscopy (Perkin Elmer Inc., Massachusetts, USA). Samples were fixed on the diamond crystal and a pressure of 90 N/cm^2 was applied to each sample. Spectra were recorded in the range from 500 to 4000 cm^{-1} and analyzed using Spectrum® Quant software.

2.3.5. Cluster compound chemical stability in aqueous nanosuspensions

Chemical stabilities of cluster compounds in CNPs were shown with 2 complementary approaches, i) their UV-visible absorption spectra evolution from preparation up to 48 hours and ii) the evolution of cluster compound concentrations in aqueous nanosuspensions during 4 weeks by UV spectroscopy at 250 nm as described in section 2.3.2. In both studies nanosuspensions were refrigerated and protected from light and measurements were performed following appropriate dilution with acetonitrile using a Specord®PC 205 UV VIS spectrophotometer (Analytik Jena AG, Jena, Germany).

2.4 *In vitro* cluster release from CNPs

Cluster compounds release analysis from nanoparticles were carried out in absolute ethanol at 25°C, respecting the "sink" condition, i.e. cluster compound solubility in the dissolution medium never exceeding 10% of its solubility. At the beginning of the experiment, 4.5ml of freshly prepared CNPs corresponding to 2 to 4 mg of cluster compounds were placed in a dialysis bag, a 25kD MWCO Spectra/Por®6 pre-wetted dialysis membrane (Spectrum Laboratories, Inc, Rancho Dominguez, CA, USA) then sealed at its 2 sides and placed in a 150 ml beaker containing 100 ml release medium with continuous magnetic stirring (250 rpm). The sampling conditions were depending on the cluster compound chemical stability in the aqueous nanosuspensions. The quick substitution of the halogen Br^- labile terminal ligands of the $[\{Mo_6Br\}_8Br_6]^{2-}$ cluster units with hydroxyl groups or water molecules described in

section 3.2 is leading to an apparent decrease in the percent released profile as a function of time. To overcome this situation, percent cluster released was obtained from the percent cluster remaining in the dialysis bag at the sampling time. At each sampling time (30, 60, 180, 360 and 1440 and 2880 min) the flask was centrifuged (5000 g /10 min) the supernatant was discarded, the nanoparticles in sediment were solubilized in 5 ml acetonitrile and the percent cluster released was evaluated by UV spectrophotometer at 250 nm after dilution (1/20) with acetonitrile using the method mentioned in section 2.3.2. For CMIF, the apical ligand substitution kinetics was much slower than for $[\{Mo_6Br\}_8Br_6]^{2-}$ cluster unit based salts and direct sampling in the donor compartment was possible at each sampling time. Each point represents the mean ± SD of 3 different batches.

2.5. Photophysical studies

Absolute photoluminescence quantum yields, ϕ_{em}, were measured on powdered cluster compounds and on CNPs (as aqueous nanosuspensions or freeze-dried solid nanoparticles) using a Hamamatsu C9920-03G measurement system (Hamamatsu Photonics France, Massy, France) comprising a xenon excitation light source, an integrating sphere and a red-sensitive multichannel photodetector Hamamatsu PMA-12. The excitation wavelength was set at 365 nm. The same Hamamatsu set up was used to obtain emission spectra.

2.6. Statistical analysis

All experiments were performed in triplicate. Results are presented as mean ± SD. Mean values of nanoparticle size, PDI, zeta potential and encapsulation efficiency were compared using the Mann and Whitney test and differences were considered significant at the level of $p < 0.05$.

3. RESULTS AND DISCUSSION

3.1. Nanoparticles formulation and characterization

PLGA nanoparticles were prepared by the solvent displacement method also known as nano-precipitation method (Fessi et al., 1989). The oily phase or organic phase is a solution of acetone in which both cluster compound and PLGA polymer are dissolved while the aqueous phase is a distilled water solution of surfactant polyoxyethylenesorbitan monolaurate. Cluster loaded polymer nanosuspensions were obtained following dropwise addition of the organic phase to the aqueous phase. Particle size is one of the most critical factor to consider for the cellular uptake of colloidal system, sizes between 50-150 nm are needed for optimal uptake by tumor cells (He et al., 2010). Following acetone removal under reduced pressure and using the preparation conditions described in section 2.2, several cluster nanoparticles (CNPs) were obtained with 3 different P/C ratios, i.e 1, 2.5 and 5. Table 1 shows the nanoparticle sizes, polydispersity indexes (PDI) and zeta potential obtained for all freshly prepared formulations. All nanoparticles sizes obtained were compatible with a cellular uptake, higher sizes were obtained with CMIF the cluster salt with the higher atomic mass and significant variations in nanoparticle sizes were observed when the tested P/C ratio was increased from 1 to 5, with sizes increasing from the range 75-100 nm (P/C = 1) to the range 120-145 nm (P/C = 5). This result is in accordance with other studieson PLGA concentration effect on nanoparticles size and this may be due to an increase of the solution viscosity (Halayqa et al., 2014; Homs et al., 2018). PDI values were always < 0.2 indicating a homogenous monodispersed profile of the prepared nanoparticles but this time a significant decrease was observed when P/C ratio was increased from 1 to 5, i.e. 33%, 77% and 33% for TBA_2, CMIF and CMB_3 respectively, indicating a narrowing of size distribution with higher P/C ratio. Zeta potentials were all comprised between -25 and -45 mV, measuring the negative electric charge on the nanoparticle surface resulting from the interaction between PLGA and the polysorbate 20 surfactant.

Zeta potential absolute values higher than 30 mV are generally related to better nanoparticle physical stabilities due to stronger electrostatic repulsion between nanoparticles (Gupta and Trivedi, 2018), the highest Zeta potential values were obtained with the P/C ratio of 2.5, whatever the cluster compound tested. The encapsulation efficiencies (EE%), cluster loadings (CL%) and mass yields (MY%) obtained for each CNPs were determined using UV spectrophotometry and the results are reported in Table 2. The EE was higher than 60% for all

P/C ratios tested indicating an efficient cluster entrapment within the nanoparticles. Among the cluster compounds tested, only CMIF-PLGA reached an EE% higher than 95%. CLs were as expected significantly decreased when P/C ratio was increased. The MY% vas evaluated after freeze-drying of the samples and no statistically significant differences were observed between the different P/C ratios tested.

TEM was performed to examine CNPs morphology. For each cluster compound tested, all P/C ratios showed the same morphology, therefore only nanoparticles with a P/C ratio of 2.5 were presented in Figure 2A. TEM images show the spherical shape and the porous structure of CNPs prepared by nanoprecipitation, the particle size, around 50 nm were always lower than those obtained with dynamic light scattering as already reported and commented in our previous study with TBA_2 (P/C = 0.5) (Brandhonneur et al., 2018). Figure 2B presents freshly prepared CNPs with a P/C ratio of 2.5 under daylight (left) and following photo-activation under UV light at 365 nm (right) exhibiting eye-observable intensive red luminescence for CMIF and less intensive pink to red luminescence, according to P/C ratio for CMB and TBA_2.

Fourier Transform Infrared spectroscopy was performed to investigate the polymer/cluster interactions resulting from the cluster encapsulation in the nanoparticles. As PLGA is an organic polymer , it is easy to follow the shifts concerning well characterized vibrations such as C=O stretching or carbonyl bond at 1750cm^{-1}, C-O ester stretching at 1088cm^{-1} and sp3 C-H stretching at 1750cm^{-1}. The results obtained for blank polymeric nanoparticles and CNPs are given in Table 3. The C=O stretch recorded for the polymer at 1750 cm^{-1} did not change in CNPs while the peak representing the C-O ester stretching slightly moved from 1088 cm^{-1} for the polymer to 1078 cm^{-1} and 1083 cm^{-1} for both molybdenum halide CNPs with a P/C ratio of 2.5, TBA_2 and CMB, respectively. The vibration corresponding to the sp3 C-H stretching was detected at 2914 cm^{-1} for the polymer and moved significantly between 2921 and 2924 cm^{-1} for all CNPs tested, indicating the existence of interactions between the polymer and the cluster compound. Nevertheless, FT-IR spectra show the presence of all polymer characteristic peaks and the absence of new chemical modifications creation following cluster compound incorporation into nanoparticles (data not presented), this clearly indicates the lack of strong chemical interactions formed but rather physical ones. This comes in accordance with other studies on PLGA nanoparticles incorporating drugs such as methotrexate, garcinol or hesperidin where authors concluded to the lack (Jang et al., 2019; Gaoncar et al., 2017) or to minor (Ali et al., 2019) chemical interaction between drug and polymer.

3.2. CNPs Physico-chemical stability

CNPs physical stability is an essential parameter in formulation. The colloidal stability of polymeric nanoparticles can be monitored by the change of particle size, PDI and zeta potential at a function of time following storage in close vials protected from light, at ambient temperature (+25°C) or refrigerated (between +2 and +8°C). For blank PLGA nanoparticles, colloidal stability was conserved during the 3 months study whatever the temperature (Supplementary material 1). Figure 3 shows the evolution of size, PDI and Zeta Potential following dynamic light scattering measurements on a 3 months storage period for the nanosuspensions refrigerated between +2 and +8°C and protected from light. Particle sizes were not statistically modified during the 3 month of storage for all cluster compounds and all P/C ratios tested, only a slight increase in size, always below 5%, was measured over the period. Identically, PDI were not significantlty modified, all values were comprised between 0.09 and 0.19, showing the conservation of size distribution over time. Zeta potential values, predictor of nanoparticles medium or long term instability, increased rapidly after nanoparticle preparation, up to 50% at day 7 and were approaching zero after 1 month. This decrease in Zeta potential values not observed with blank nanoparticles may be related to cluster compound hydrolysis and the creation of new chemical species perturbing the nanoparticles environment thus limiting CNPs physical stability to 3 months under refrigeration. These rapid decrease of zeta potential values were also confirmed when the nanosuspensions were stored at ambient temperature (25 ± 1°C) and protected from light (Supplementary material 2) but this time, size was significantly increased after 2 months for TBA_2 (8 fold increase) and CMB (2 fold increase) loaded nanoparticles only with P/C ratio of 1, while size was not modified during the period for CMIF. We can conclude that i) keeping the nanosuspensions refrigerated is delaying the manifestation of instability; ii) zeta potential is a critical parameter to predict a forthcoming instability; iii) increasing polymer concentration improves nanoparticle stability and iv) using pentafluoro propionate as organic apical ligand instead of brome seems to protect nanoparticles from aggregation. Chemical stabilities of cluster compounds were also checked by following the evolution of absorption spectra of aqueous nanosuspensions and by determination of cluster compounds concentrations in nanosuspensions by UV spectroscopy at 250 nm. The UV-visible absorption spectra of freshly prepared nanosuspensions of TBA_2, CMIF and CMB, as well as their evolution for 48h (at 0, 3, 6, 24 and 48 hours) were recorded in acetonitrile and are shown in figure 4. For CMIF all spectra from 0 to 48 hours are superposed signing the lack of chemical

modification during the period studied while for the 2 other clusters with brome as apical ligand, the intensity of the UV absorption maximum around 250 nm was continually decreasing during the same period and for TBA_2 a second UV absorption peak near 217 nm was increasing, corresponding to the formation of a new chemical compound as shown with the isosbestic point at 230 nm. In fact, molybdenum cluster compounds are known to be unstable in water where they are converted into aqua hydroxo complexes by substitution of labile apical ligand by hydroxyl groups or water molecules leading to micron sized aggregates with altered luminescence properties (Daigre et al., 2018; Kirakci et al., 2016, 2019; Svezhentseva et al., 2017). Encapsulating the cluster in a matrix such as SiO_2 nanoparticles (Aubert et al., 2013), polystyrene microparticles (Efremova et al., 2014) or nanoassemblies with betacyclodextrins (Kirakci et al., 2014) was shown to be a solution to circumvent the tendency to easily hydrolyse in water. In our study the use of a porous biocompatible polymeric matrix is interesting with fluoropropionate organic apical ligand, as seen with CMIF that can, contrary to halogen ligand protect the Mo_6I_8 cluster core from water hydrolysis and this was also observed with a similar cluster core with fluorinated apical ligand presented as colloidal nanodispersion (Kirakci et al., 2018). This was also confirmed by the UV assay of cluster compound in the nanoparticles during 4 weeks (figure 5).

The percent cluster compound remaining unchanged at a function of time from CNPs was better for CMIF (lack of cluster loss after one week; <10% loss after 4 weeks) than for the two other cluster compounds, TBA_2 (10% and 30% loss after 1 and 4 weeks, respectively) and CMB (30% and > 50% loss after 1 and 4 weeks, respectively). This time again CMIF was the most protected within the PLGA matrix for up to 4 weeks due to the shielding effect of the organic apical ligand.

As shown in our previous study, release of cluster compound from CNPs is needed for an optimal activity following photo-activation (Brandhonneur et al., 2018). Figure 6 presents the percent cluster released as a function of time for the 3 clusters and the 3 P/C ratios. As mentioned in material and methods section, *in vitro* release was performed in ethanol to respect the sink condition for the duration of the test. From percent released curves we can see a high initial burst for each cluster compound with more than 50% released at 180 min for all P/C ratios, followed by a prolonged release phase during the 48h test. The initial quantity released by burst effect is decreasing with P/C ratio for all cluster compounds, from 60-65% (P/C = 1) to 50% (P/C = 5) and this can be explained by the mechanisms of cluster release from PLGA nanoparticles that are drug diffusion in the porous matrix happening from the beginning followed by late polymer degradation by ester linkages hydrolysis. The cluster

compound diffusion is improved with low P/C ratio due to a smaller polymeric matrix. In the same way, the lower the P/C ratio (i.e.1), the higher the percent released at 24h, i.e. 88%, 80% and 75% for CMIF, CMB and TBA_2, respectively and the higher the P/C ratio (i.e. 5), the lower the percent released at 24h, i.e. 71%, 71% and 60%, for CMIF, CMB and TBA_2, respectively. It is also possible to compare the different profiles by estimating the time needed to obtain 50% of release or $t_{50\%}$, and this parameter was always increasing with P/C ratio, i.e. from 77.2 to 138.9 min, 150.2 to 185.2 min and 24.8 to 171.2 min for CMIF, CMB and TBA_2, respectively, when P/C ratio was increased from 1 to 5. There was a slight effect of P/C ratio on the release of the cluster compound from nanoparticles, it seems that only a higher P/C ratio that was not studied in this work (i.e > 5) could significantly decrease the release of the encapsulated cluster compound thus affecting the production of singlet oxygen following photoactivation.

3.3. Photophysical properties

Molybdenum cluster compound are known to exhibit photoluminescence between 550 and 900 nm with quantum yield up to 100% and luminescence lifetimes up to 400 µs (Vorotnikov et al., 2017; Kirakci et al., 2012; Efremova et al., 2016; Maverick et al., 1983). When metal cluster compounds are embedded into a polymeric matrix there is a need to check if the photophysical properties of the starting cluster compound are affected. For that purpose we compared the luminescence properties of the molybdenum cluster compounds before and after their incorporation into PLGA matrixes. Photophysical parameters for powdered pure cluster compounds CMB, TBA_2 or CMIF and for their PLGA nanoparticulate systems presented in Figures 7, 8 and 9 (emission spectra) and Table 4 (photoluminescence absolute quantum yields or AQY). The irradiation of CNPs in the UV-Blue region is leading to the cluster emission in the red-near infrared (from 550 to 900 nm). Emission spectra were recorded from CNPs nanosuspensions and from solid state CNPs obtained after freeze drying of the nanosuspensions. From emission spectra (Figures 7, 8 and 9) we can observe a broad emission signal typical of metal clusters phosphorescence when they are irradiated in the UV-blue region at 365 nm. Cluster compound incorporation in PLGA matrix does not lead to a modification of the general shape of its emission band, only a slight blue shift of emission signal could be guessed when CNPs were dispersed in water compared with their solid form, but no significant shift of the emission maximum (figure 7). A slight red shift of cluster

compound emission maximum (15 nm) could only be seen with CMIF following its incorporation into PLGA nanoparticles but no emission maximum shift could be detected when P/C ratio was modified (Figure 8). All these results are evidencing that cluster compounds emission properties are preserved when they are embedded into PLGA nanoparticles.

AQY depend on the ratio of the emission and the absorption energy and thus characterize the ability of a sample to emit light following irradiation. An increase in the emission signal intensity was observed with CMIF loaded nanoparticles (P/C ratio = 2.5) when passing from an air to a N_2 saturated atmosphere in the integrating sphere (Figure 9) and this phenomenon was reversible when N_2 was replaced by air. Octahedral clusters compound excited state are known to efficiently react with triplet oxygen to form emissive singlet oxygen (Jackson et al., 1990), resulting in a quenching of the cluster emission signal, i.e. its luminescence. The decrease in atmosphere dioxygen concentration obtained with N_2 resulted in a decrease of cluster luminescence quenching. This phenomenon is a totally reversible physical phenomenon that does not lead to a chemical alteration of the emitting cluster, as seen with the lack of emission maximum shift. Incorporation of molybdenum clusters in polymeric PLGA network led to a decrease of AQY (Table 4) and this was also reported with several cluster compounds, $((C_4H_9)_4N)_2[(Mo_6I_8)(NO_3)_6)]$ (Vorotnikov et al., 2016), $((C_4H_9)_4N)_2[\{Mo_6I_8\}(CF_3CO_2)_6)]$ (Kirakci et al., 2012) and CMB (Aubert et al., 2013; Grasset et al., 2008) following their incorporation into SiO_2 micro or nanoparticles and was also reported for Mo_6 clusters after incorporation in PMMA (Amela-Cortes et al., 2016) or PMMA-PEOMA copolymer (Robin et al., 2018) matrixes, these modifications being attributed to perturbation of the ligand environment in the polymeric matrix or to cluster compound instability during nanoparticles preparation, i.e. apical ligand substitution by water molecules. The highest values were obtained for pure cluster compounds in solid state compared to CNPs and, as reported by Amela-Cortes at al. (2015, 2016), molybdenum cluster compound with organic apical ligand (CMIF) gave the higher AQY compared to clusters with halogen apical ligands (CMB and TBA_2). AQY values were not significantly increased with cluster compound concentration (i.e. when decreasing P/C ratio) showing that cluster compound were absorbing most of the light at the excitation wavelength used, i.e. 365 nm. Because of the existence of interactions between the triplet excited state of cluster compounds and molecular oxygen, aerated water nanosuspensions were poorly emissive, as seen with AQY values of 6.6, 1.5 and 2% for TBA_2, CMIF and CMB, respectively. For this reason

AQY values in freshly prepared nanosuspension were lower than those in solid state, excepted for CMIF for which no difference was seen between nanosuspension and solid form, the organic ligand giving a slightly higher protection against the quenching of luminescence by dioxygen. The luminescence quenching could also be reversed as seen with AQY value raising from 1.3 to 28% following 15 min N_2 bubbling of CMIF solid loaded nanoparticles. From this study we can conclude that intrinsic properties of molybdenum cluster compound are not significantly modified when they are incorporated in PLGA nanoparticles.

Conclusion

Molybdenum cluster salts were successfully incorporated in PLGA matrixes leading to homogenous cluster loaded nanosuspensions characterized as efficient delivery systems. All nanoparticles had sizes compatible with cellular uptake, could quickly release their embedded cluster compound and exhibited good colloidal stabilities upon refrigeration. However, the tendency of cluster compounds to hydrolysis in water resulted in poor cluster chemical stability especially when the apical ligand was a halogen, limiting the shelf-life of the cluster loaded nanosuspensions. Thus, the development of a dry dosage form to be reconstituted extemporaneously before injection, capable to maintain cluster salts physico-chemical as well as photo-chemical properties for a longer period is of paramount importance. As cluster compounds photophysical properties are preserved when they are embedded into PLGA nanoparticles, their initial values are important to take into account before considering a biological application such as PDT. *In vitro* biological properties of these CNPs, i.e. cellular uptake, toxicity and photoactivity on ovarian cancer cells are currently under investigation.

Acknowledgements

Emission lifetime measurements were performed with CAPHTER Platform facilities (SCANMAT, UMS 2001 CNRS-University of Rennes 1) which received financial support from Rennes Metropole and European Union (CPER-FEDER 2015-2020, project CAPHTER). Ludivine Rault is acknowledged for TEM observations performed at THEMIS (ScanMAT, UMS 2001 CNRS - University of Rennes 1). The authors thank Noée Dumait (UMR 6226 University of Rennes 1) for cluster compound synthesis.

References

Ahmed, N., Fessi, H., Elaissari, A., 2012. Theranostic applications of nanoparticles in cancer. Drug Discovery Today, 17, 928-934. https://doi.org/10.1016/j.drudis.2012.03.010

Ali, S.H., Sulaiman, G.M., Al-Halbosiy, M.M.F., Jabir, M.S., Hameed, A.H., 2019. Fabrication of hesperidin nanoparticles loaded by poly lactic co-Glycolic acid for improved therapeutic efficiency and cytotoxicity. Artificial cells, Nanomedecine and Biotechnology, 47, 378-394. https://doi.org/10.1080/21691401.2018.1559175

Amela-Cortes, M., Garreau, A., Cordier, S., Faulques, E., Duvail, JL, Molard, Y., 2014. Deep red luminescent hybrid copolymer materials with high transition metal cluster content. J. Mat. Chem. C, 2,1545-1552. https://doi.org/10.1039/c3tc31309c

Amela-Cortes, M., Paofai, S., Cordier, S., Folliot, H., Molard, Y., 2015. Tuned red NIR phosphorescence of polyurethane hybrid composites embedding metallic nanoclusters for oxygen sensing. Chem. Commun.,51, 8177-8180. https://doi.org/10.1039/c5cc01867f

Amela-Cortes, M., Molard, Y., Paofai, S., Desert, A., Duvail, J-L., Naumov, N.G., Cordier, S., 2016. Versatility of the ionic assembling method to design highly luminescent PMMA nanocomposites containing $[M_6Q_8^iL_6^a]^{n-}$ octahedral nano-building blocks. Dalton Trans., 45, 237-245. https://doi.org/10.1039/c5dt03734d

Aubert, T., Cabello-Hurtado, F., Esnault, M-A., Neaime, C., Lebret-Chauvel, D., Jeanne, S., Pellen, P., Roiland, C., Le Polles, L., Saito, N., Kimoto, K., Haneda, H., Ohashi, N., Grasset, F., Cordier, S., 2013. Extended investigations on luminescent Cs2[Mo6Br14]@SiO2

499 nanoparticles: physico-structural characterizations and toxicity studies. J. Phys. Chem. C, 117,
500 20154-20163. https://doi.org/10.1021/jp405836q

501 Brandhonneur, N., Hatahet, T., Amela-Cortes, M., Molard, Y., Cordier, S., Dollo, G., 2018.
502 Molybdenum cluster loaded PLGA nanoparticles: an innovative theranostic approach for the
503 treatment of ovarian cancer. Eur. J. Pharm. Biopharm., 125, 95-105. https://doi.org/
504 10.1016/j.ejpb.2018.01.007

505 Costuas, K., Garreau, A., Bulou, A., Fontaine, B., Cuny, J., Gautier, R., Mortier, M., Molard,
506 Y., Duvail, J.-L., Faulques, E., Cordier, S., 2015. Combined theoretical and time-resolved
507 photoluminescence investigations of $[Mo_6Br^i_8Br^a_6]^{2-}$ metal cluster units: evidences of multi-
508 component emission. Phys. Chem. Chem. Phys., 17, 28574-28585.
509 https://dx.doi.org//10.1039/c5cp03960f

510 Daigre, J., Cuny, P., Lemoine, M., Amela-Cortes, S. Paofai, N. Audebrand, A. Le Gal La
511 Salle, E. Quarez, O. Joubert, N. G. Naumov, S. Cordier, 2018. Metal-Atom clusters as
512 building blocks for multifunctional proton-conducting materials: theoretical and experimental
513 characterization. Inorg. Chem., 57, 9814-9825.https://doi.org/10.1021/acs.inorgchem.8b00340

514 Dierre, B., Costuas, K., Dumait, N., Paofai, S., Amela-Cortes, M., Molard, Y., Grasset, F.,
515 Cho, Y., Takahashi, K., Ohashi, N., Uchikoshi, T., Cordier, S., 2017. Mo_6 cluster-based
516 compounds for energy conversion applications: comparative study of photoluminescence and
517 cathodoluminescence. Science and Technology of Advanced Materials. 18, 458–466.
518 https://doi.org/10.1080/14686996.2017.1338496

519 Efremova, O.A., Shestopalov, M.A., Chirtsova, N.A., Smolentsev, A.I., Mironov, Y.V.,
520 Kitamura, N., Brylev, K.A., Sutherland, A.J., 2014. A highly emissive inorganic
521 hexamolybdenum cluster complex as a handy precursor for the preparation of new
522 luminescent materials. Dalton Trans., 43, 6021-6025. https://doi.org/ 10.1039/c3dt53126k

523 Efremova, O.A., Vorotnikov, Y.A., Brylev, K.A., Vorotnikova, N.A., Novozhilov, I.N.,
524 Kuratieva, N.V., Edeleva, M.V., Benoit, D.M., Kitamura, N., Mironov, Y.V., Shestopalov,
525 M.A., Sutherland, A.J., 2016. Octahedral molybdenum cluster complexes with aromatic
526 sulfonate ligands. Dalton Trans., 45, 15427-15435. https://doi.org/ 10.1039/c6dt02863b

527 Fessi, H., Puisieux, F., Devissaguet, J-P., Ammoury, N., Benita, S., 1989. Nanocapsule

formation by interfacial polymer deposition following solvent displacement. Int.J. Pharm. 55, R1-R4. https://doi.org/10.1016/0378-5173(89)90281-0

Francois, G., Katz, J.L., 2005. Nanoparticles and nanocapsules created using the Ouzo effect: spontaneous emulisification as an alternative to ultrasonic and high-shear devices, Chemphyschem., 6, 209-216. https://doi.org/10.1002/cphc.200400527

Gaonkar, R.H., Ganguly, S., Dewanjee, S., Sinha, S., Gupta, A., Ganguly, S., Chattopadhyay, D.,; Chatterjee Debnath, M., 2017. Garcinol loaded vitamin E TPGS emulsified PLGA nanoparticles: preparation, physicochemical characterization, *in vitro* and in vivo studies. Sci. Rep.,7, 530. https://doi.org/10.1038/s41598-017-00696-6

Grasset, F., Dorson, F., Cordier, S., Molard, Y., Perrin, C., Marie, A-M., Sasaki, T., Haneda, H., Bando, Y., Mortier, M., 2008. Water-in-oil microemulsion preparation and characterization of $Cs_2[Mo_6X_{14}]$ @SiO_2 phosphor nanoparticles based on transition metal clusters (X=Cl, Br, I), Adv. Mater., 20, 143-148. https://doi.org/10.1002/adma.200701686

Gupta, V., Trivedi, P., 2018. *In vitro* and *in vivo* characterization of pharmaceutical topical nanocarriers containing anticancer drugs for skin cancer treatment, in: Grumezescu, A.M. (Ed), Lipid nanocarriers for drug targeting. William Andrew applied Science Publisher, pp. 563-627. https://doi.org/10.1016/c2016-0-04170-0

Halayqa, M., Domanska, U., 2014. PLGA biodegradable nanoparticles containing perphenazine or chlorpromazine hydrochloride: effect of formulation and release, Int. J. Mol. Sci., 15, 23909-23923. https://doi.org/ 10.3390/ijms151223909

He, C., Hu, Y., Yin, L., Tang, C., Yin, C., 2010. Effects of particle size and surface charge on cellular uptake and biodistribution of polymeric nanoparticles, Biomaterials 31, 3657-3666. https://doi.org/10.1016/j.biomaterials.2010.01.065

Homs, M., Caldero, G., Monge, M., Morales, D., Solans, C., 2018. Influence of polymer concentration on the properties of nanoemulsions and nanoparticles obtained by a low-energy method, Colloids and surfaces A: physicochemical and engineering aspects, 536, 204-212. https://doi.org/10.1016/j.colsurfa.2017.06.009

Jackson, J.A., Turro, C., Newsham, M.D., Nocera, D.G., 1990. Oxygen quenching of

556 electronically excited hexanuclear molybdenum and tungsten halide clusters, J. Physic.
557 Chem., 94, 4500-4507. https://doi.org/10.1021/j100374a029

558 Jackson, J.A., Newsham, M.D., Worsham, C., Nocera, D.G., 1996. Efficient singlet oxygen
559 generation from polymers derivatized with hexanuclear molybdenum clusters, Chem. Mater.,
560 8, 558-564. https://doi.org/10.1021/cm950443f

561 Jang, J.H., Jeong, S.H., Lee Y.B., 2019. Preparation and *in vitro*/*in vivo* characterization of
562 polymeric nanoparticles containing methotrexate to improve lymphatic delivery, Int. J. Mol.
563 Sci., 20, 3312. https://doi.org/10.3390/ijms20133312

564 Kirakci, K., Cordier, S., Perrin C., 2005. Synthesis and characterization of $Cs_2Mo_6X_{14}$ (X= Br
565 or I) hexamolybdenumcluster halides: efficient Mo_6 cluster precursors for solution chemistry
566 syntheses, Z. Anorg. Allg. Chem., 631, 411-416. https://doi.org/10.1002/zaac.200400281

567 Kirakci, K., Kubát, P., Dušek, M., Fejfarová, K., Šícha, V., Mosinger, J., Lang, K., 2012. A
568 highly luminescent hexanuclear molybdenum cluster - a promising candidate toward
569 photoactive materials, Eur. J. Inorg. Chem., 19, 3107-3111. https://doi.org /10.1002/ejic.
570 201200402

571 Kirakci, K., Kubát, P., Kučeráková, M., Šícha, V., Gbelcová, H., Lovecká, P., Grznárová, P.,
572 Ruml, T., Lang, K., 2016. Water-soluble octahedral molybdenum cluster compounds
573 $Na_2[Mo_6I_8(N_3)_6]$ and $Na_2[Mo_6I_8(NCS)_6]$: Syntheses, luminescence, and *in vitro* studies,
574 Inorganica Chimica Acta, 441, 42-49. https://doi.org /10.1016/j.ica.2015.10.043

575 Kirakci, K., Zelenka, J., Rumlová, M., Martincik, J., Nikl, M., Ruml, T., Lang K., 2018.
576 Octahedral molybdenum cluster as radiosensitizers for X-ray induced photodynamic therapy,
577 J. Mater. Chem. B, 6, 4301-4307. https://doi.org /10.1039/c8tb00893k

578 Kirakci, K., Zelenka, J., Rumlová, M., Cvačka, J., Ruml, T., Lang K., 2019. Cationic
579 octahedral molybdenum cluster complexes functionalized with mitochondria-targeting
580 ligands: photodynamic anticancer and antibacterial activities, Biomater. Sci., 7, 1386-1392.
581 https://doi.org /10.1039/c8bm01564c

582 Maverick, A.W., Najdzionek, J.S., MacKenzie, D., Nocera, D.G., Gray, H.B., 1983.
583 Spectroscopic, electrochemical, and photochemical properties of molybdenum (II) and

584 tungsten (II) halide clusters, J. Am. Chem. Soc., 105, 1878-1882. https://doi.org
585 /10.1021/ja00345a034

586 Nayak, S.K., Amela-Cortes, M., Roiland, C., Cordier, S., Molard, Y., 2015. From metallic
587 cluster-based ceramics to nematic hybrid liquid crystals: a double supramolecular approach,
588 Chem. Commun., 51, 3774-3777. https://doi.org /10.1039/c4cc10085

589 Neaime, C., Amela-Cortes, M., Grasset, F., Molard, Y., Cordier, S., Dierre, B., Mortier, M.,
590 Takei, T., Takahashi, K., Haneda, H., Verelst, M., Lechevallier, S., 2016. Time-gated
591 luminescence bioimaging with new luminescent nanocolloids based on $[Mo_6I_8(C_2F_5COO)_6]^{2-}$
592 metal atom clusters, Phys. Chem. Chem. Phys., 18, 30166-30173. https://doi.org/
593 10.1039/c6cp05290h

594 Robin, M., Dumait, N., Amela-Cortes, M., Roiland, C., Harnois, M., Jacques, E., Folliot, H.,
595 Molard, Y., 2018. Direct integration of red-NIR emissive ceramic-like $A_nM_6X^i_8X^a_6$ metal
596 cluster salts in organic copolymers using supramolecular interactions, Chemistry, 24, 4825-
597 4829. https://doi.org/10.1002/chem.201800860

598 Solovieva, A.O., Vorotnikov, Y.A., Trifonova, K.E., Efremova, O.A., Krasilnikova, A.A.,
599 Brylev, K.A., Vorontsova, E.V., Avrorov, P.A., Shestopalova, L.V., Poveshchenko, A.F.,
600 Mironovand, Y.V., Shestopalov, M.A., 2016. Cellular internalisation, bioimaging and dark
601 and photodynamic cytotoxicity of silica nanoparticles doped by $\{Mo_6I_8\}^{4+}$metal clusters, J.
602 Mater. Chem. B, 4, 4839. https://doi.org/10.1039/c6tb00723f

603 Svezhentseva, E.V., Solovieva, A.O., Vorotnikov, Y.A., Kurskaya, O.G., Brylev, K.A.,
604 Tsygankova, A.R., Edeleva, M.V., Gyrylova, S.N., Kitamura, N., Efremova, O.A.,
605 Shestopalov, M.A., Mironov Y.V., Shestopalov, A.M., 2017. Water-soluble hybrid materials
606 based on $\{Mo_6X_8\}^{4+}$ (X = Cl, Br, I) cluster complexes and sodium polystyrene sulfonate, New
607 J. Chem., 41, 1670-1676. https://doi.org/10.1039/c6nj03469a

608 Vorotnikov, Y.A., Solovieva, A.O., Trifonova, K.E., Efremova, O.A., Chirtsova, N.A.,
609 Brylev, K.A., Krasilnikova, A.A., Edeleva, M.V., Tsygankova, A.R., Smolentsev, A.I.,
610 Vorontsova, E.V., Avrorov, P.A., Shestopalova, L.V., Kitamura, N., Poveshchenko, A.F.,
611 Mironov, Y.V., Shestopalov, M.A., 2016. On the synthesis, characterization and biological
612 properties of luminescent hybrid particles: Mo_6 metal cluster/SiO_2, RCS Adv. 6, 43367-
613 43375. https://doi.org/10.1039/c6ra04321f

614 Vorotnikov, Y.A., K.E., Efremova, O.A., Novozhilov, I.N., Yanshole, V.V., Kuratieva, N.V.,
615 Brylev, K.A., Kitamura, N., Mironov, Y.V., Shestopalov, M.A., 2017. Hexaazide octahedral
616 molybdenum cluster complexes: Synthesis, properties and the evidence of hydrolysis, Journal
617 of Molecular Structure, 1134, 237-243. https://doi.org/10.1016/j.molstruc.2016.12.052

618 Vorotnikova, N., Edeleva, M., Kurskaya, O., Brylev, K., Shestopalov, A., Mironov, Y.,
619 Sutherland, A., Efremova O., Shestopalov, M., 2017. One-pot synthesis of $\{Mo_6 I_8\}^{4+}$doped
620 polystyrene microspheres via a free-radical dispersion copolymerisation reaction. Polymer
621 International, 10, 5473. https://doi.org/10.1002/pi.5473

622 Vorotnikova, N.A., Alekseev, A. Y., Vorotnikov, Y. A., Evtushok, D. V., Molard, Y., Amela-
623 Cortes, M., Cordier, S., Smolentsev, A. I., Burton, C. G., Kozhin, P., M., Zhu, P., Topham, P.
624 D., Mironov, Y.V., Bradley, M., Efremova, O.A., Shestopalov, M.A., 2019. Octahedral
625 molybdenum cluster as a photoactive antimicrobial additive to a fluoroplastic. Materials
626 Science & Engineering C, 105, 110150–110150. https://doi.org/10.1016/j.msec.2019.110150

627

Figure captions

Figure 1. General structure of hexanuclear molybdenum halide cluster unit ($Mo_6L^i_8L^a_6$) where L^i and L^a represent inner (Br or I in our study) and apical (Br or $(OOC_2F_5)_6$ in our study) ligands, respectively and A^+ represents the counter cation ($((C_4H_9)_4N^+$ = TBA^+ or Cs^+ in our study).

Figure 2. Characterization of CNPs (P/C ratio = 2.5). A) TEM images of TBA_2 (left), CMIF (middle) and CMB (right) and B) photographs of water suspensions under daylight (left images / yellow colour) and UV light at 365 nm (right images / red phophorescence) for TBA_2 (left), CMIF (middle) and CMB (right).

Figure 3. Water suspended CNPs stability upon 3 months storage at 4°C and protected from light. Blank columns show particle size results, PDI are shown as lines and filled columns show zeta potential values (each bar is the mean ± SD of 3 determinations).

Figure 4. Water suspended CNPs UV-visible spectra evolution as a function of time (hour) for TBA_2, CMIF and CMB (P/C ratio = 2.5).

Figure 5. Percent cluster compound remaining unchanged at a function of time from water suspended CNPs with P/C ratios of 1 and 2.5.

Figure 6. *In vitro* release study of cluster compound TBA2, CMIF and CMB from water suspended CNPs with 3 different P/C ratios. Each point represents the mean ± SD of 3 differents batches.

Figure 7. Emission spectra recorded at λ_{exc}= 365 nm for TBA_2 in powder (black signal) and for TBA_2 loaded nanoparticles (P/C ratio = 2.5) as nanosuspension in water (greysignal) or solid form following freeze-drying of the nanosuspension (light grey signal).

Figure 8. Left: Solid state emission spectra of CMIF (black) and CMIF loaded nanoparticles (P/C ratio = 2.5) (grey); Right: Solid state emission spectra of CMIF loaded nanoparticles with 3 different P/C ratios.

Figure 9. Evolution of emission signal recorded at λ_{exc}= 365 nm for solid CMIF loaded nanoparticles (P/C = 2.5) with saturation of atmosphere with N_2

***Conflict of Interest**

Declaration of interests

☒ The authors declare that they have no known competing financial interests or personal relationships that could have appeared to influence the work reported in this paper.

☐The authors declare the following financial interests/personal relationships which may be considered as potential competing interests:

Table 1

	Size (nm)	PDI	Zeta Potentiel (mV)
TBA_2 - PLGA[a]	85.7 ± 4.9	0.12 ± 0.02	-25.8 ± 4.4
CMIF - PLGA[a]	102.0 ± 2.6	0.16 ± 0.01	-38.2 ± 1.7
CMB - PLGA[a]	75.7 ± 2.5	0.16 ± 0.02	-22.4 ± 9.8
TBA_2 - PLGA[b]	95.0 ± 6.1	0.12 ± 0.01	-42.2 ± 8.0
CMIF - PLGA[b]	124.7 ± 2.5	0.08 ± 0.02	-47.8 ± 4.6
CMB - PLGA[b]	99.3 ± 4.6	0.12 ± 0.01	-47.8 ± 9.1
TBA_2 - PLGA[c]	141.7 ± 6.4	0.09 ± 0.02	-24.8 ± 1.3
CMIF - PLGA[c]	144.7 ± 4.7	0.09 ± 0.03	-31.5 ± 3.6
CMB - PLGA[c]	118.3 ± 4.3	0.12 ± 0.01	-43.1 ± 6.5

P/C ratio **a)** 1; **b)** 2.5 and **c)** 5

Table 1. Size (nm), polydispersity index (PDI) and zeta-potential (ZP) for all water suspended CNPs with 3 different P/C ratios (each value is the mean ± SD of 3 determinations).

Table 2

	EE %	CL	MY %
TBA_2 - PLGA[a]	63.1 ± 7.5	50.9 ± 3.5	78.1 ± 10.2
CMIF - PLGA[a]	68.1 ± 5.2	73.6 ± 12.9	83.1 ± 12.8
CMB - PLGA[a]	61.7 ± 6.3	73.9 ± 9.4	69.2 ± 4.1
TBA_2 - PLGA[b]	85.6 ± 12.1	38.0 ± 13.5	76.2 ± 4.8
CMIF - PLGA[b]	96.3 ± 1.8	69.8 ± 6.5	78.4 ± 7.0
CMB - PLGA[b]	70.3 ± 7.8	47.8 ± 12.0	67.7 ± 18.8
TBA_2 - PLGA[c]	60.3 ± 4.5	29.2 ± 5.6	79.5 ± 7.1
CMIF - PLGA[c]	96.9 ± 2.3	55.0 ± 9.4	81.0 ± 2.2
CMB - PLGA[c]	81.4 ± 6.8	34.9 ± 3.0	72.1 ± 11.2

P/C ratio **a)** 1; **b)** 2.5 and **c)** 5

Table 2. EE%, CL and MY% for all CNPs with 3 different P/C ratios (each value is the mean ± SD of 3 determinations).

Table 3

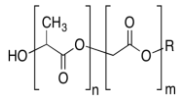	**C=O stretching 1749 cm^{-1}**	**C-0 ester stretching 1088 cm^{-1}**	**Sp3 C-H bond 2914 cm^{-1}**
TBA_2 - PLGA[a]	1752	1088	**2924**
CMIF - PLGA[a]	1750	1084	**2922**
CMB - PLGA[a]	1751	1085	**2921**
TBA_2 - PLGA[b]	1752	**1080**	**2923**
CMIF - PLGA[b]	1752	1084	**2922**
CMB - PLGA[b]	1751	**1083**	n.d.
TBA_2 - PLGA[c]	1750	1084	**2924**
CMIF - PLGA[c]	1749	1084	**2923**
CMB - PLGA[c]	1750	1084	**2923**

P/C ratio **a)** 1; **b)** 2.5 and **c)** 5; n.d: result not determined
Bold values mean significant shifts

Table 3. FT-IR vibrations obtained with PLGA blank nanoparticles characteristic bonds and their mofification following cluster loading in PLGA nanoparticles.

Table 4

	λ_{em} (nm)	ϕ_{em} solid state (in air)	ϕ_{em} water suspension (aerated)
TBA_2	785	0.22[a]	n.d.
TBA_2 - NP 1	785	0.120	0.066
TBA_2 - NP 2.5	785	0.137	0.066
TBA_2 - NP 5	785	0.143	0.067
CMIF	660	0.35[b]	n.d.
CMIF - NP 1	675	0.013	0.014
CMIF - NP 2.5	675	0.013	0.016
CMIF - NP 5	675	0.017	0.016
CMB	767	0.14[c]	n.d.
CMB - NP 1	767	0.032	0.020
CMB - NP 2.5	767	0.032	0.019
CMB - NP 5	767	0.038	0.020

[a, b, c]: values obtained previously in our team (same experimental conditions and apparatus) by Amela-Cortes (2014), Robin (2018) and Nayak (2015), respectively.

Table 4. Emission maximum wavelengths (λ_{em}) and absolute quantum yield (ϕ_{em}) values obtained at λ_{exc} = 365 nm for cluster compounds in solid state and CNPs in solid state or as nanosuspension in water.

Figure 1

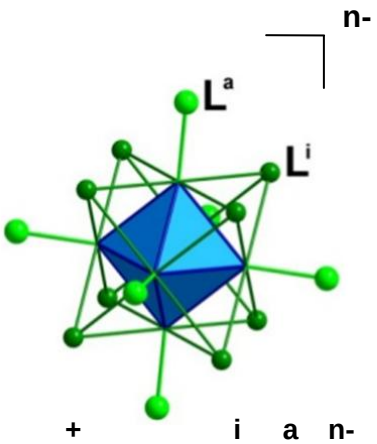

$$(A^{+})_n\,[Mo_6L^{i}_{8}L^{a}_{6}]^{n-}$$

Figure 2

A)

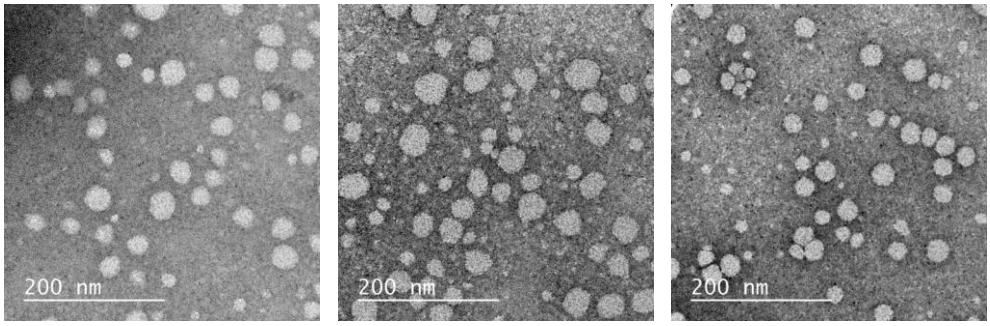

B)

Figure 3

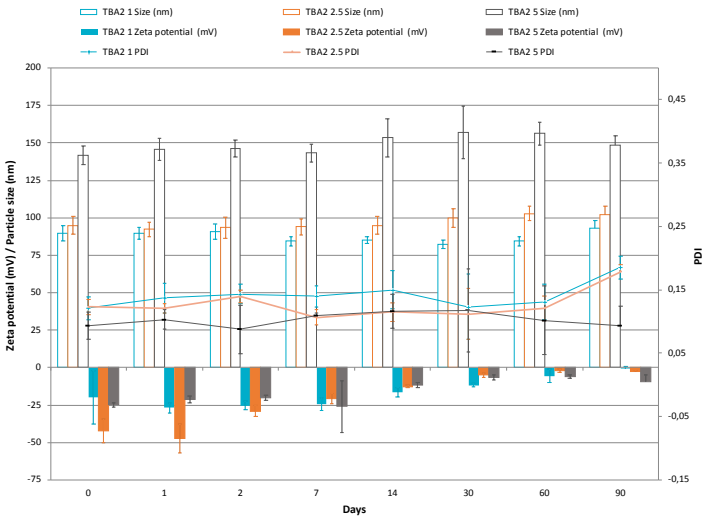
TBA2 1 Size (nm)
TBA2 2.5 Size (nm)
TBA2 5 Size (nm)
TBA2 1 Zeta potential (mV)
TBA2 2.5 Zeta potential (mV)
TBA2 5 Zeta potential (mV)
TBA2 1 PDI
TBA2 2.5 PDI
TBA2 5 PDI
Zeta potential (mV) / Particle size (nm)
PDI
Days
0
1
2
7
14
30
60
90

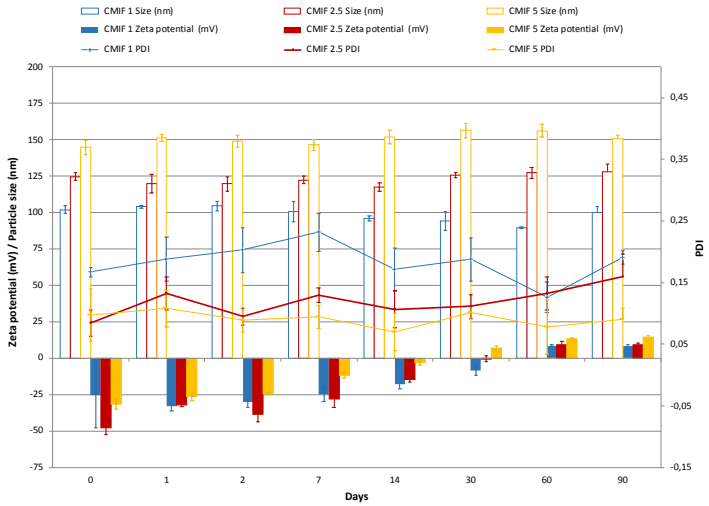
CMIF 1 Size (nm)
CMIF 2.5 Size (nm)
CMIF 5 Size (nm)
CMIF 1 Zeta potential (mV)
CMIF 2.5 Zeta potential (mV)
CMIF 5 Zeta potential (mV)
CMIF 1 PDI
CMIF 2.5 PDI
CMIF 5 PDI
Zeta potential (mV) / Particle size (nm)
PDI
Days
0
1
2
7
14
30
60
90

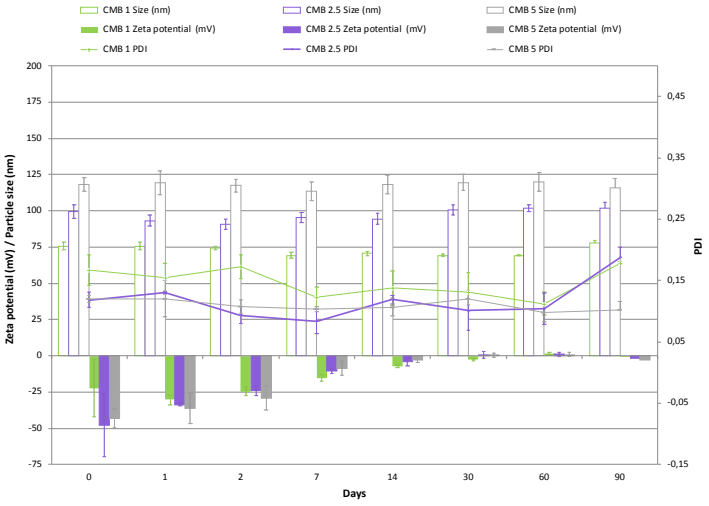
CMB 1 Size (nm)
CMB 2.5 Size (nm)
CMB 5 Size (nm)
CMB 1 Zeta potential (mV)
CMB 2.5 Zeta potential (mV)
CMB 5 Zeta potential (mV)
CMB 1 PDI
CMB 2.5 PDI
CMB 5 PDI
Zeta potential (mV) / Particle size (nm)
PDI
Days
0
1
2
7
14
30
60
90

Figure 4

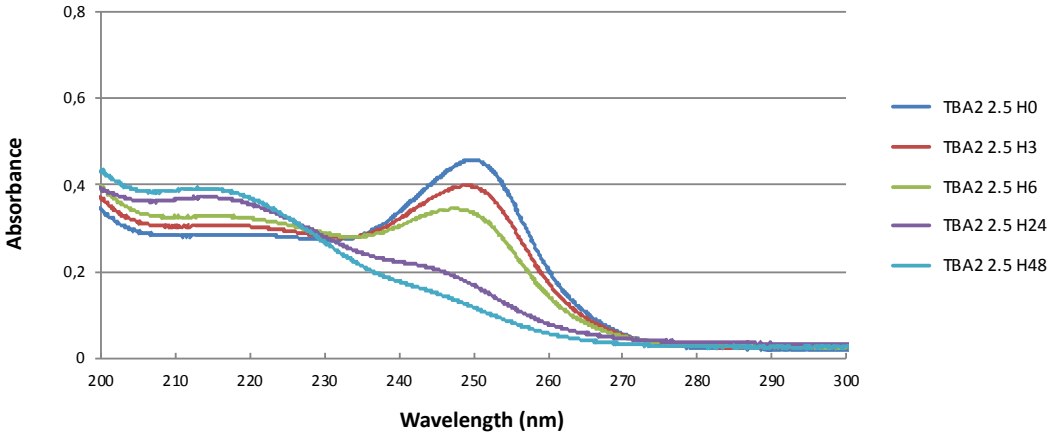
0,8
0,6
0,4
0,2
0
Absorbance
200 210 220 230 240 250 260 270 280 290 300
Wavelength (nm)
TBA2 2.5 H0
TBA2 2.5 H3
TBA2 2.5 H6
TBA2 2.5 H24
TBA2 2.5 H48

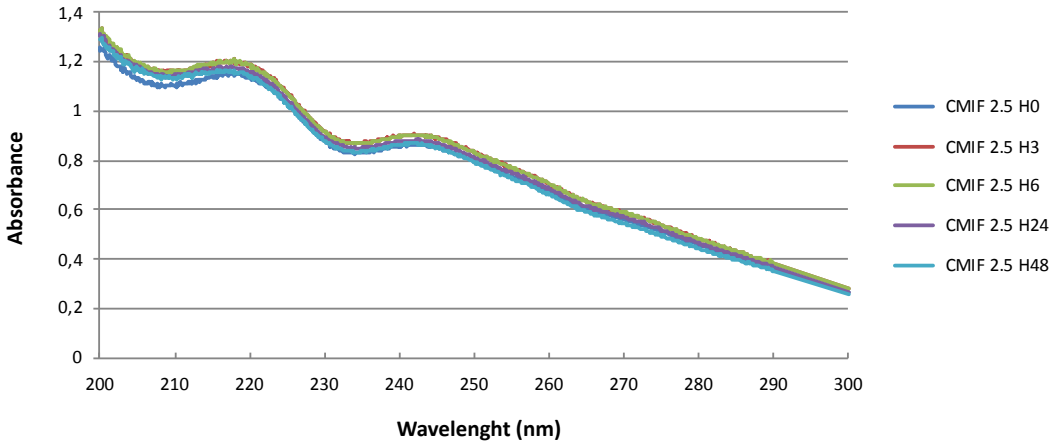
1,4
1,2
1
0,8
0,6
0,4
0,2
0
Absorbance
200 210 220 230 240 250 260 270 280 290 300
Wavelenght (nm)
CMIF 2.5 H0
CMIF 2.5 H3
CMIF 2.5 H6
CMIF 2.5 H24
CMIF 2.5 H48

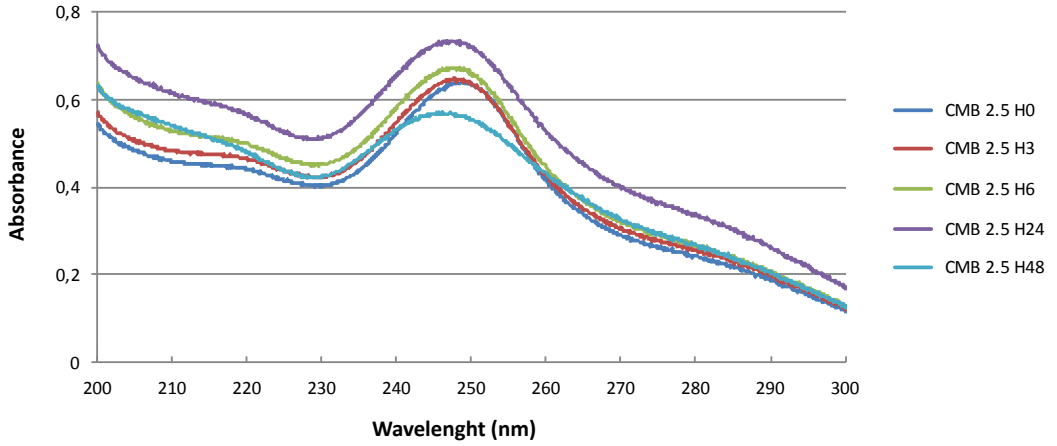
0,8
0,6
0,4
0,2
0
Absorbance
200 210 220 230 240 250 260 270 280 290 300
Wavelenght (nm)
CMB 2.5 H0
CMB 2.5 H3
CMB 2.5 H6
CMB 2.5 H24
CMB 2.5 H48

Figure 5

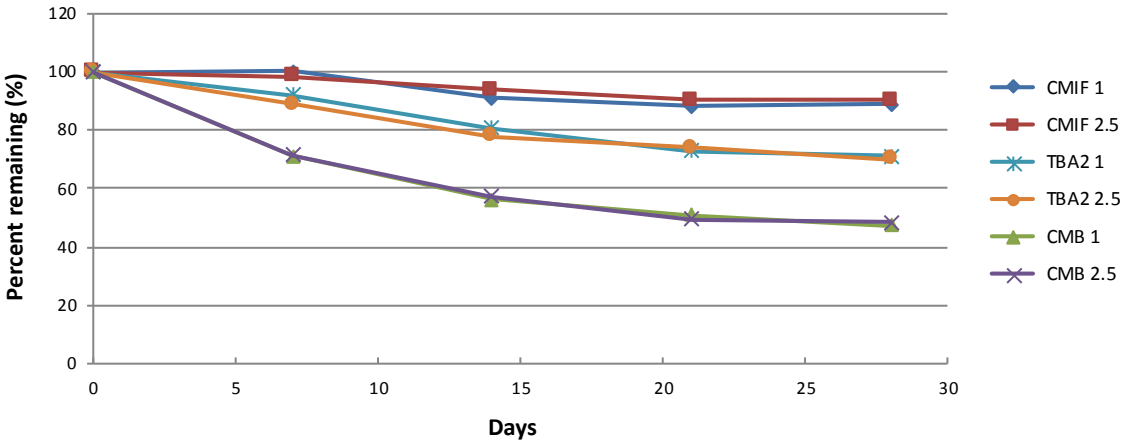
120
100
80
60
40
20
0
Percent remaining (%)
0
5
10
15
20
25
30
Days
CMIF 1
CMIF 2.5
TBA2 1
TBA2 2.5
CMB 1
CMB 2.5

Figure 6

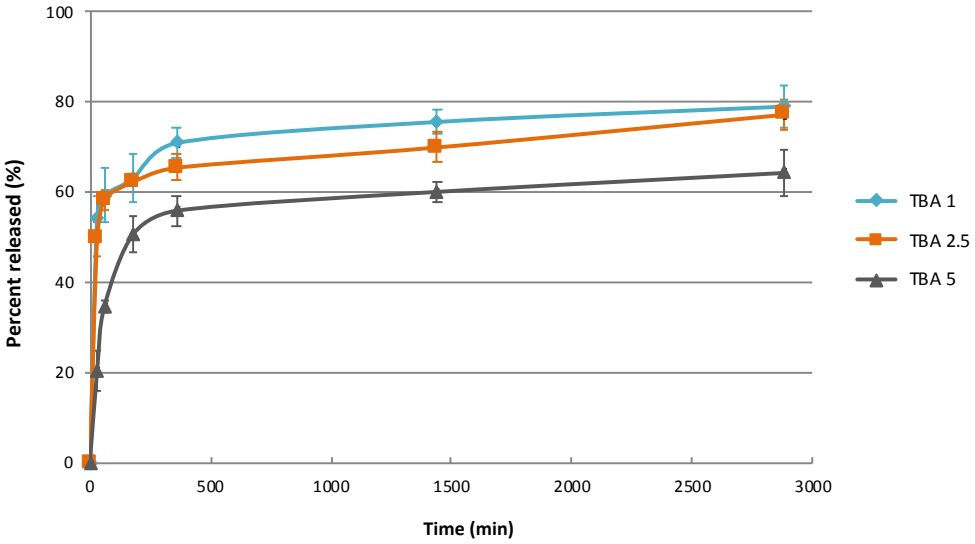
100
80
60
40
20
0
Percent released (%)
0
500
1000
1500
2000
2500
3000
Time (min)
TBA 1
TBA 2.5
TBA 5

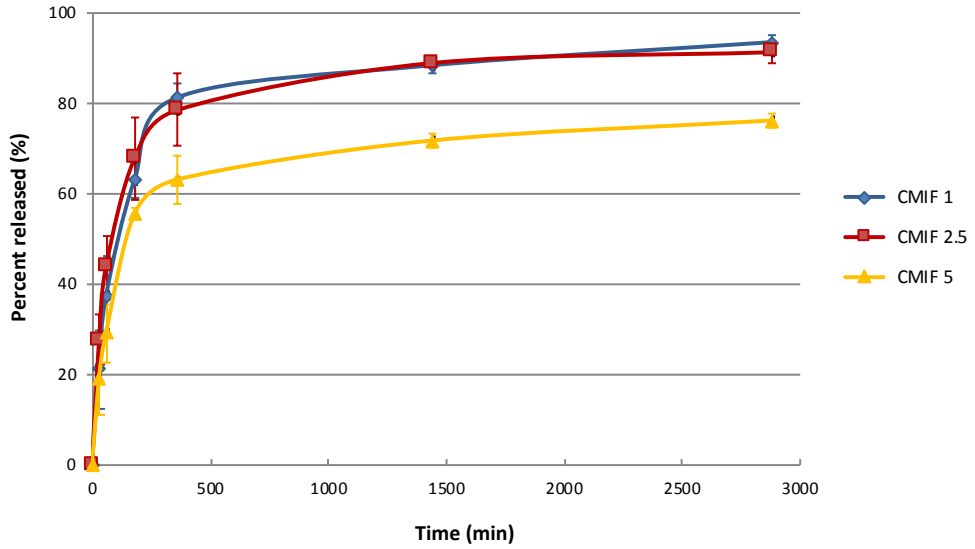
100
80
60
40
20
0
Percent released (%)
0
500
1000
1500
2000
2500
3000
Time (min)
CMIF 1
CMIF 2.5
CMIF 5

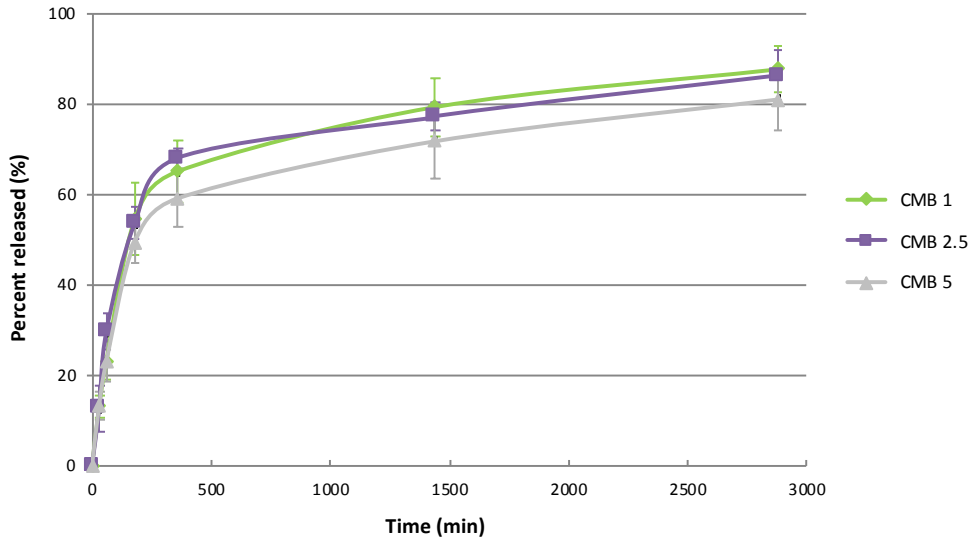
100
80
60
40
20
0
Percent released (%)
0
500
1000
1500
2000
2500
3000
Time (min)
CMB 1
CMB 2.5
CMB 5

Figure 7

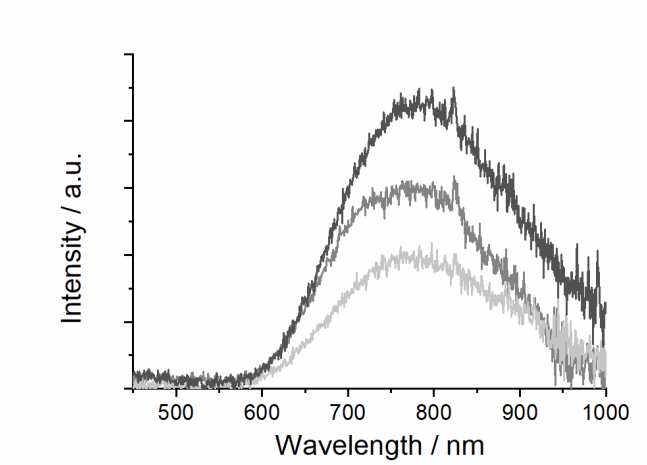

Figure 8

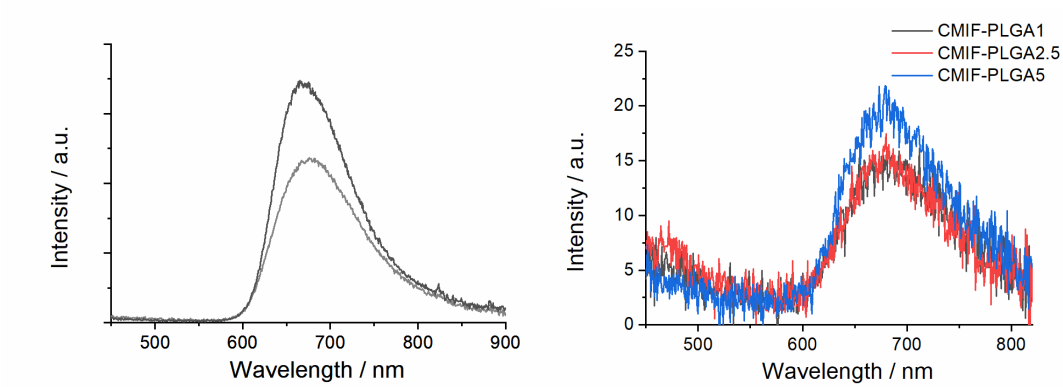
Intensity / a.u.
500
600
700
800
900
Wavelength / nm
CMIF-PLGA1
CMIF-PLGA2.5
CMIF-PLGA5
Intensity / a.u.
0
5
10
15
20
25
500
600
700
800
Wavelength / nm

Figure 9

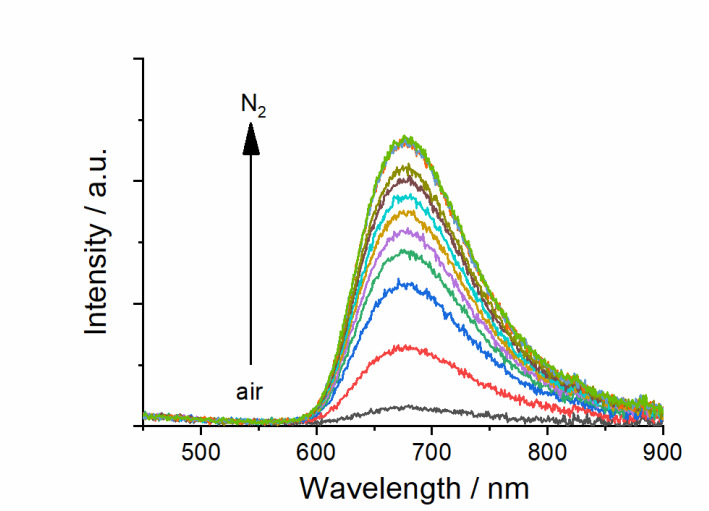

Supplementary Material

Click here to download Supplementary Material: supplementary material.docx